Inorganic Chemistry

Article

pubs.acs.org/IC

Variable-Rung Design for a Mixed-Valence Two-Legged Ladder System Situated in a Dimensional Crossover Region

Kazuya Otsubo,*[,†,‡] Atsushi Kobayashi,[§] Kunihisa Sugimoto,[∥] Akihiko Fujiwara,[∥] and Hiroshi Kitagawa*[,†,‡,⊥,▽]

[†]Division of Chemistry, Graduate School of Science, Kyoto University, Kitashirakawa Oiwake-cho, Sakyo-ku, Kyoto 606-8502, Japan

[‡]Core Research for Evolutional Science and Technology (CREST), Japan Science and Technology Agency (JST), 7 Goban-cho, Chiyoda-ku, Tokyo 102-0075, Japan

[§]Division of Chemistry, Faculty of Science, Hokkaido University, Kita-10, Nishi-8, Kita-ku, Sapporo 060-0810, Japan

[∥]Japan Synchrotron Radiation Research Institute (JASRI), SPring-8, 1-1-1 Kouto, Sayo-cho, Sayo-gun, Hyogo 679-5198, Japan

[⊥]Institute for Integrated Cell-Material Sciences (iCeMS), Kyoto University, Yoshida, Sakyo-ku, Kyoto 606-8501, Japan

[▽]INAMORI Frontier Research Center, Kyushu University, 744 Motooka, Nishi-ku, Fukuoka 819-3095, Japan

Supporting Information

ABSTRACT: Ladder systems situated in a crossover from one dimensionality to two dimensionalities have been an attractive research target, because the physical properties, which are associated with dimensionality, are strongly dependent on the number of constituent legs. However, control of the intraladder configuration and electronic properties based on the substitution of structural components remain challenging tasks in materials science. On the other hand, structural design using coordination chemistry offers crucial advantages for architectural and electronic variations through substitutions of metal−organic building blocks. Here, we show the rational design and electronic properties of novel metal complex-based two-legged ladder compounds with several organic rung units: 4,4′-bipyridine, trans-1,4-diaminocyclohexane, and 4,4′-azopyridine. Single-crystal X-ray studies show that these two-legged ladder compounds are composed of halogen-bridged mixed-valence one-dimensional chains (MX chains) as their constituent legs. Depending on the molecular shape of the organic rung units, unique configurations of two-legged ladder lattices with periodic distortion of the legs are achieved. In addition, the electronic absorption spectra show that intervalence charge-transfer (IVCT) band gap of the two-legged ladder system increases with increasing degree of distortion of the leg. We have demonstrated for the first time that a two-legged ladder system shows a unique relationship between IVCT energy and the distortion parameter of the leg, as distinct from a single MX chain system. These systematic investigations, not only of configurations based on the rung variation but also of electronic states in metal−organic ladder system, provide the possibility for wide and rational tunings of physical and electronic properties of metal complex-based functional materials.

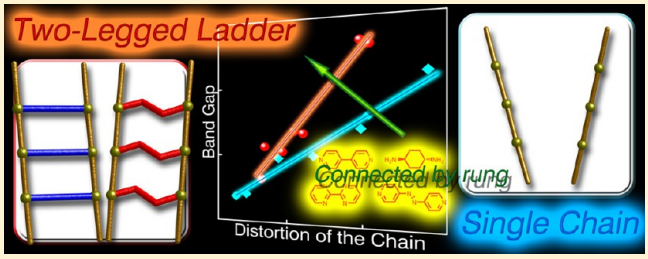

INTRODUCTION

Dynamical electronic states induced by mixed valency offer a wide variety of interesting physical properties in the solid state, such as metallic conduction, superconductivity, and charge-density-wave (CDW), and spin-density-wave (SDW) states.[1] In particular, low-dimensional electronic systems as represented by one-dimensional (1-D) chain systems have attracted much attention, because of a range of characteristic physical properties such as nonlinear optical properties, Mott insulation, Peierls instability, solitons, and polarons resulting from the strong fluctuations derived from a subtle balance of electronic energies, such as transfer integral (t), onsite (U), and intersite (V) Coulomb repulsions, and electron−lattice interaction (S).[2]

Among the low-dimensional electronic systems, ladder materials have been of particular research interest during the past few decades. Because the electronic properties of mixed-valence 1-D chain systems are dominated by strong (or weak) intra- and interchain electronic correlations, the ladder system is expected to be an ideal research target that exists in the dimensional crossover between 1-D and two-dimensional (2-D) electronic systems. Actually, transition-metal oxide ladder systems have attracted significant attention from a wide range of scientists because of their unique magnetic and electronic properties, superconductivity, and quantum phenomena being strongly dependent on the number of constituent legs.[3] However, precise and intentional control of the number of legs, intraladder configurations based on the variations of leg and rung, and electronic states of the oxide ladder compounds are generally difficult, because of their extreme synthetic

Received: November 13, 2013
Published: January 6, 2014

   dx.doi.org/10.1021/ic402846v | Inorg. Chem. 2014, 53, 1229−1240

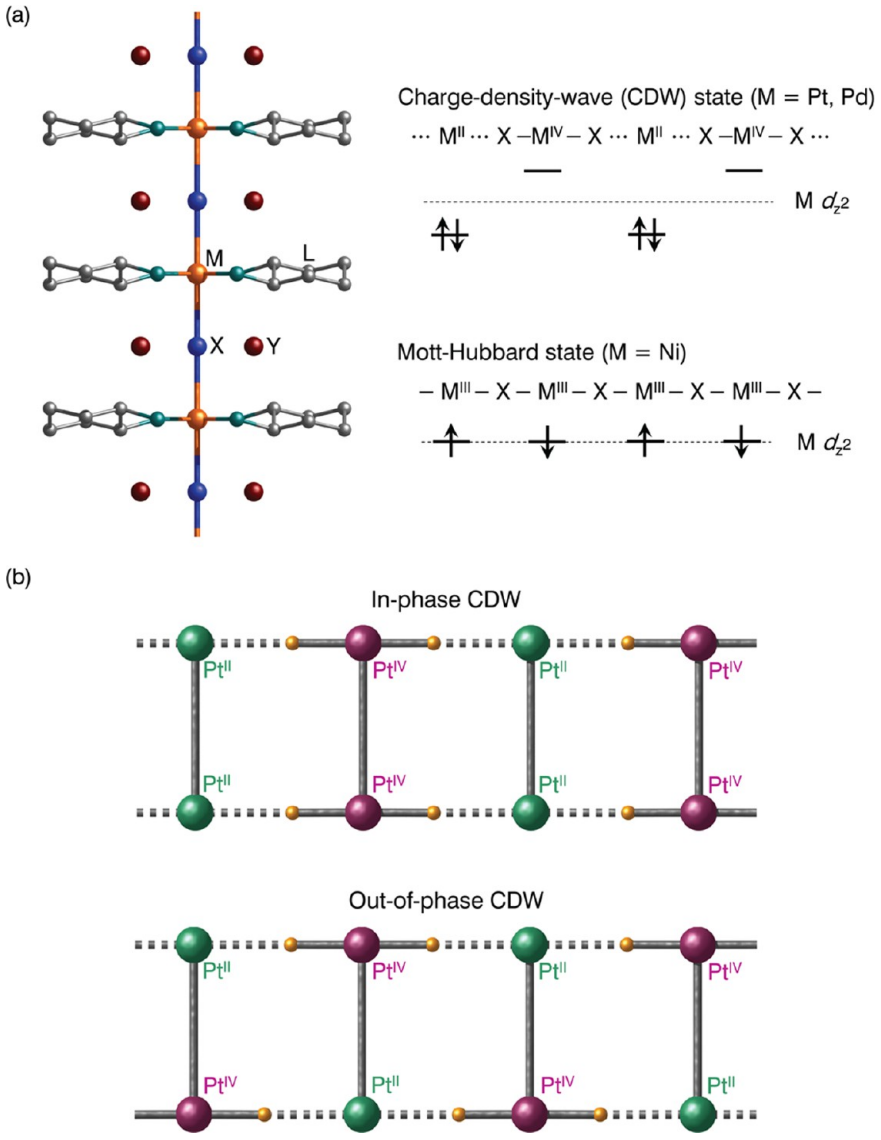

Figure 1. (a) Typical 1-D chain structure and two types of possible electronic ground states with their relative M d_z^2 orbital energy levels in the MX chain system. M, X, L, and Y denote the central metal ion, bridging halide ion, organic terminal ligand, and counteranion, respectively. (b) Two types of valence arrangements found in the two-legged MX ladder system. (For details, see ref 6.)

conditions (i.e., high temperature, etc.). In addition, these ladders are mainly composed of metal and oxide ions, where the oxide-bridged metal unit and the oxide ion itself constitute the leg and rung, respectively. This situation also results in a lack of structural and electronic variations.

In view of such shortcomings of oxide ladder systems, fabrication of nanosized architecture based on the coordination bond has crucial advantages not only for structural designability and regularity, but also for variation of electronic properties through substitution of structural components such as metal ions, organic ligands, and counterions.[4] Because of this, halogen-bridged mixed-valence ladder systems are currently of particular interest as novel metal complex-based ideal isolated ladder materials. In these compounds, 1-D halogen-bridged mixed-valence mononuclear metal complexes, comprising the so-called MX chain,[5] constitute the leg, and organic ligands combine several MX chains as rungs to form an isolated ladder lattice (i.e., MX ladder). By utilizing coordination chemistry to develop such nanoarchitectures, several two-legged ladder-type[6] and four-legged tube-type[7] MX ladder systems have recently been achieved.

The single MX chain family is a classical material that shows unique electronic states and physical properties, such as luminescence with a large Stokes shift, resonant Raman scattering with overtone progressions, long-range migration of solitons and polarons, and large third-order nonlinear optical susceptibility due to the dynamical electronic system.[5] Electronic ground states of MX chain compounds are classified into two types: CDW and Mott−Hubbard states, depending on the metal species, as shown in Figure 1a. Their electronic properties can be controlled via substitution of structural components such as metal ions, bridging-halide ions, organic ligands, and counterions. Because the MX chain family has high tunability, as mentioned above, novel MX ladder systems have been expected to offer a high number of structural and electronic degrees of freedom.[6,7] Actually, MX ladder systems show unique electronic properties induced by interchain electronic interactions through the organic rung ligand, which are quite different from those of a single MX chain system, for

dx.doi.org/10.1021/ic402846v | Inorg. Chem. 2014, 53, 1229−1240

Scheme 1. Structural Variation of Two-Legged Ladder System via Rung Selection

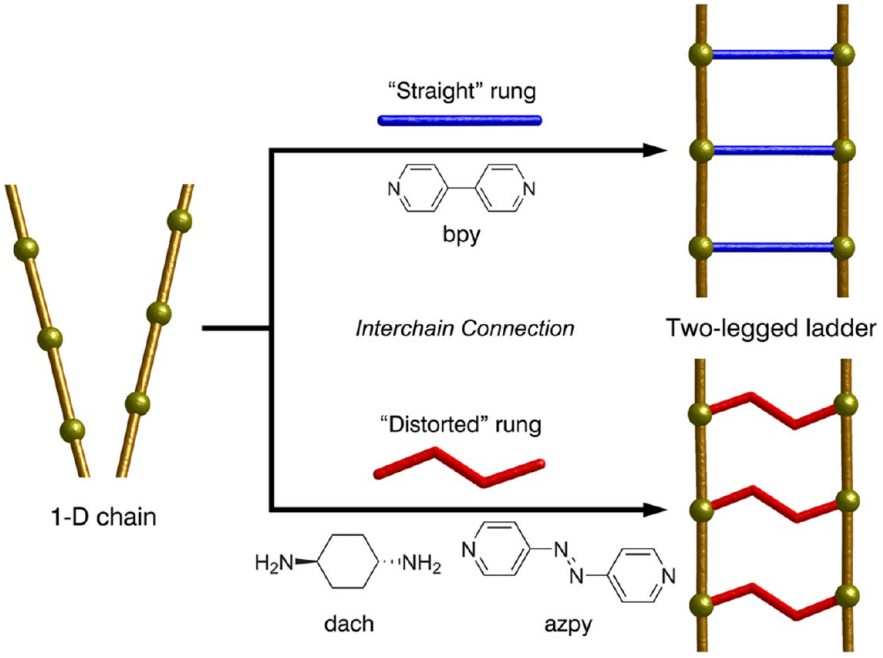

example, pairs of in-phase[6a] and out-of-phase[6b] CDW states within the ladder have been realized in some two-legged MX ladder compounds (Figure 1b). In addition, in the case of four-legged MX-tube-type compound, these interchain ordered valence arrangements are induced among the adjacent four MX chains accompanying the increased number of MX legs.[7] Such unique electronic states based on the interchain correlation have not been observed in the single MX chain system, implying that the rung units play an important role for the electronic states of the MX ladder system. However, the effects of the rung unit on structural and electronic properties of the MX ladder system still remain unknown because there is only a handful of examples of MX ladder compounds, and their constituent rung units are limited to two types of "straight" and "rigid" organic molecules (4,4′-bipyridine (bpy), 2,2′-bipyrimidine (bpym)). In this work, we have focused on structural and electronic variations based on the rung substitution in the two-legged MX ladder system. To achieve this, trans-1,4-diaminocyclohexane (dach) and 4,4′-azopyridine (azpy), which have a "distorted" molecular shape, were selected as rungs from structural points of view (Scheme 1). We expected that these substitutions could convey the advantages for the rational design of structural and electronic properties of metal complex-based ladder materials, compared with oxide ladder systems.

In this article, we describe the structural design, crystal structures, and electronic states of novel halogen-bridged two-legged MX ladder compounds with three different organic rung units: bpy, dach, and azpy. Two MX chains are connected by organic rung units, forming a two-legged ladder lattice, where the MX chains are the leg. We have successfully introduced distorted organic rungs into two-legged MX ladder system. One of the obtained MX ladder compounds has a straight rung (bpy) with unique "zigzag"-shaped MX legs, and the others are unprecedented compounds having distorted rungs (dach and azpy) where the overall configurations of the two-legged ladder lattice are distorted. Moreover, for the first time, we have demonstrated that the two-legged MX ladder system shows a distinct tendency for its intervalence charge-transfer (IVCT) band gap to depend strongly on the distortion of the MX leg, which is quite different from that of single MX chain system.

EXPERIMENTAL SECTION

Reagents and solvents were purchased from Wako Pure Chemical Industries, Ltd., TCI Co., Ltd., Alfa Aesar Co., and Sigma–Aldrich Chemical Co., and used without further purification.

Synthesis of $\{[PtBr(dien)]_2(bpy)\}(NO_3)_4\cdot 2H_2O$ (1, dien = diethylenetriamine, bpy = 4,4′-bipyridine). Starting materials, $\{[Pt(dien)]_2(bpy)\}(NO_3)_4$ and $\{[PtBr_2(dien)]_2(bpy)\}Br_4$ were prepared according to the previous report.[6b] A water/methanol (2:3) solution containing $\{[Pt(dien)]_2(bpy)\}(NO_3)_4$ (20 mg, 0.020 mmol) and $\{[PtBr_2(dien)]_2(bpy)\}Br_4$ (28 mg, 0.020 mmol) was carefully layered on a water/methanol solution (1:1) containing an excess amount of $(CH_3)_4NNO_3$ (1.5 g, 11 mmol) in a capped test tube (25 mL) at room temperature (rt). Needle-shaped blue single crystals of **1** were obtained after three weeks (yield: 18 mg, 50%). Elemental analysis (%). Calcd for $C_{18}H_{34}Br_2N_{12}O_{12}Pt_2\cdot 2H_2O$: C, 18.07; H, 3.20; N, 14.05. Found: C, 18.13; H, 3.62; N, 14.23.

Synthesis of $\{[Pt(dien)]_2(dach)\}(NO_3)_4$ (dach = trans-1,4-diaminocyclohexane). $[Pt(dien)](NO_3)_2$ (260 mg, 0.62 mmol) was added to 60 mL of methanol solution containing dach (36 mg, 0.32 mmol). After reflux for a day, the resulting solution was cooled to rt, and the pale gray precipitate was collected by filtration and dried in vacuo (yield: 271 mg, 91%). Slow evaporation of an aqueous solution of this precipitate afforded plate-shaped colorless single crystals suitable for X-ray crystallography.[8] Elemental analysis (%). Calcd for $C_{14}H_{40}N_{12}O_{12}Pt_2$: C, 17.54; H, 4.21; N, 17.53. Found: C, 17.26; H, 4.11; N, 17.33.

Synthesis of $\{[PtBr_2(dien)]_2(dach)\}Br_4\cdot 4H_2O$. $\{[Pt(dien)]_2(dach)\}(NO_3)_4$ (200 mg, 0.21 mmol) was added to 140 mL of methanol solution containing Br_2 (2 mL). After refluxing for two days, the resulting mixture was cooled to rt, and the yellow precipitate was collected by filtration and dried

dx.doi.org/10.1021/ic402846v | Inorg. Chem. 2014, 53, 1229–1240

Table 1. Crystallographic Data for 1, 2, and 3

	1	2	3
formula	$C_{18}H_{38}Br_2N_{12}O_{14}Pt_2$	$C_{14}H_{40}Br_2N_{12}O_{12}Pt_2$	$C_{21}H_{40}Cl_6N_{10}O_{17}Pt_2$
formula weight	1196.60	1118.53	1307.50
temperature (K)	100(2)	100(2)	100(2)
wavelength (Å)	0.71073	0.71073	0.71073
crystal system	monoclinic	orthorhombic	triclinic
space group	$P2_1/c$ (No. 14)	*Pbam* (No. 55)	$P\bar{1}$ (No. 2)
a (Å)	17.910(3)	15.0812(17)	9.1522(13)
b (Å)	11.4097(18)	18.109(2)	10.9649(16)
c (Å)	17.050(3)	5.5828(6)	38.500(5)
α (°)	90	90	90.0170(10)
β (°)	108.587(2)	90	90.0110(10)
γ (°)	90	90	90.0440(10)
V (Å^3)	3302.4(9)	1524.7(3)	3863.6(10)
Z	4	2	4
calcd density (g/cm^3)	2.407	2.436	2.248
μ (mm^{-1})	10.964	11.860	7.732
F(000)	2272	1060	2520
crystal size (mm^3)	0.30 × 0.20 × 0.05	0.35 × 0.05 × 0.03	0.28 × 0.07 × 0.03
θ_{min}, θ_{max} (°)	1.20, 27.37	1.76, 27.39	1.06, 27.50
total reflections	17108	7993	42497
unique reflections	7235	1865	16909
R_{int}	0.0440	0.0173	0.0274
goodness-of-fit	1.058	1.071	1.299
R_1, wR_2 [$I > 2\sigma(I)$]	0.0550, 0.1528	0.0277, 0.0777	0.0537, 0.1088
R_1, wR_2 (all reflections)	0.0613, 0.1632	0.0289, 0.0790	0.0685, 0.1139
max, min $\Delta\rho$ (e Å^{-3})	5.266, −3.755	1.808, −1.737	1.699, −2.163

in air (yield: 252 mg, 84%). Elemental analysis (%). Calcd for $C_{14}H_{40}Br_8N_8Pt_2{\cdot}4H_2O$: C, 11.83; H, 3.40; N, 7.88. Found: C, 11.82; H, 3.22; N, 7.74.

Synthesis of {[PtBr(dien)]$_2$(dach)}(NO$_3$)$_4$ (2). The synthetic procedure for **2** is almost the same as that for **1**. A water/methanol (2:3) solution containing {[Pt(dien)]$_2$(dach)}(NO$_3$)$_4$ (19 mg, 0.020 mmol) and {[PtBr$_2$(dien)]$_2$(dach)}Br$_4{\cdot}4H_2O$ (28 mg, 0.020 mmol) was carefully layered on a water/methanol solution (1:1) containing an excess amount of $(CH_3)_4NNO_3$ (1.5 g, 11 mmol) in a capped test tube (25 mL) at rt. Needle-shaped blue single crystals of **2** were obtained after two weeks (yield: 31 mg, 69%). Elemental analysis (%). Calcd for $C_{14}H_{40}Br_2N_{12}O_{12}Pt_2$: C, 15.03; H, 3.60; N, 15.03. Found: C, 14.94; H, 3.45; N, 14.77.

Synthesis of {[Pt(dien)]$_2$(azpy)}(NO$_3$)$_4{\cdot}2H_2O$ (azpy = 4,4′-azopyridine). [Pt(dien)](NO$_3$)$_2$ (238 mg, 5.47 mmol) was added to 70 mL of methanol solution containing azpy (52 mg, 0.28 mmol). The mixture was refluxed for two days. The resulting solution was cooled to rt, and the solvent was removed under reduced pressure. The red precipitate was collected by filtration using diethyl ether and dried in vacuo (yield: 233 mg, 94%). Acetone vapor was allowed to diffuse slowly into an aqueous solution of this precipitate. Needle-shaped red single crystals suitable for X-ray crystallography[8] were obtained after several days. Elemental analysis (%). Calcd for $C_{18}H_{34}N_{14}O_{12}Pt_2{\cdot}2H_2O$: C, 20.31; H, 3.60; N, 18.42. Found: C, 20.09; H, 3.36; N, 18.52.

Synthesis of {[PtCl$_2$(dien)]$_2$(azpy)}(NO$_3$)$_4$. An aqueous solution (10 mL) of {[Pt(dien)]$_2$(azpy)}(NO$_3$)$_4{\cdot}2H_2O$ (200 mg, 0.19 mmol) was treated with Cl_2, and stirred at 70 °C for two days. A pale red precipitate was obtained by slow evaporation of this solution under reduced pressure (yield: 205 mg, 92%). Acetone vapor was allowed to diffuse slowly into an aqueous solution of this precipitate. Prism-shaped red single crystals suitable for X-ray crystallography[8] were obtained after several days. Elemental analysis (%). Calcd for $C_{18}H_{34}N_{14}O_{12}Cl_4Pt_2$: C, 18.47; H, 2.93; N, 16.75. Found: C, 18.44; H, 2.99; N, 16.52.

Synthesis of {[PtCl(dien)]$_2$(azpy)}(ClO$_4$)$_4{\cdot}C_3H_6O$ (3). $HClO_4$ (70%, 3 mL) was added to aqueous solution (5 mL) containing {[Pt(dien)]$_2$(azpy)}(NO$_3$)$_4{\cdot}2H_2O$ (20 mg, 0.019 mmol) and {[PtCl$_2$(dien)]$_2$(azpy)}(NO$_3$)$_4$ (22 mg, 0.019 mmol) at rt. A yellow precipitate was gradually formed and collected by filtration after a day (yield: 36 mg, 76% calculated based on {[PtCl(dien)]$_2$(azpy)}(ClO$_4$)$_4$). Acetone vapor was allowed to diffuse slowly into aqueous solution of this precipitate. Needle-shaped yellow single crystals of **3** were obtained after a week. Elemental analysis (%). Calcd for $C_{18}H_{34}N_{10}O_{16}Cl_6Pt_2{\cdot}C_3H_6O$: C, 19.29; H, 3.08; N, 10.71. Found: C, 19.28; H, 3.20; N, 10.78. *Caution!: Because perchlorate salts are potentially explosive, sample* **3** *should be carefully handled in small amounts.*

Elemental Analyses. Elemental analyses for all compounds were performed using a Yanaco MT-5 and MT-6 CHN recorders at the Center for Elementary Analysis, Kyoto University.

Single-Crystal X-ray Crystallography. X-ray crystal structure analyses of **1**, **2**, and **3** were carried out using a Bruker SMART APEX II CCD detector with graphite-monochromated Mo Kα radiation (λ = 0.71073 Å) at 100 K. The single crystals were mounted on glass fibers. The structures were solved by direct methods (SIR2004 for **1** and **3**, SIR92 for **2**)[9,10] and expanded using Fourier techniques (DIRDIF99),[11] and refined by full-matrix least-squares refinement on F^2 (SHELXL-97),[12] using the CrystalStructure software package.[13] Refinement results for **1**, **2**, and **3** are summarized in Table 1.

dx.doi.org/10.1021/ic402846v | *Inorg. Chem.* 2014, 53, 1229−1240

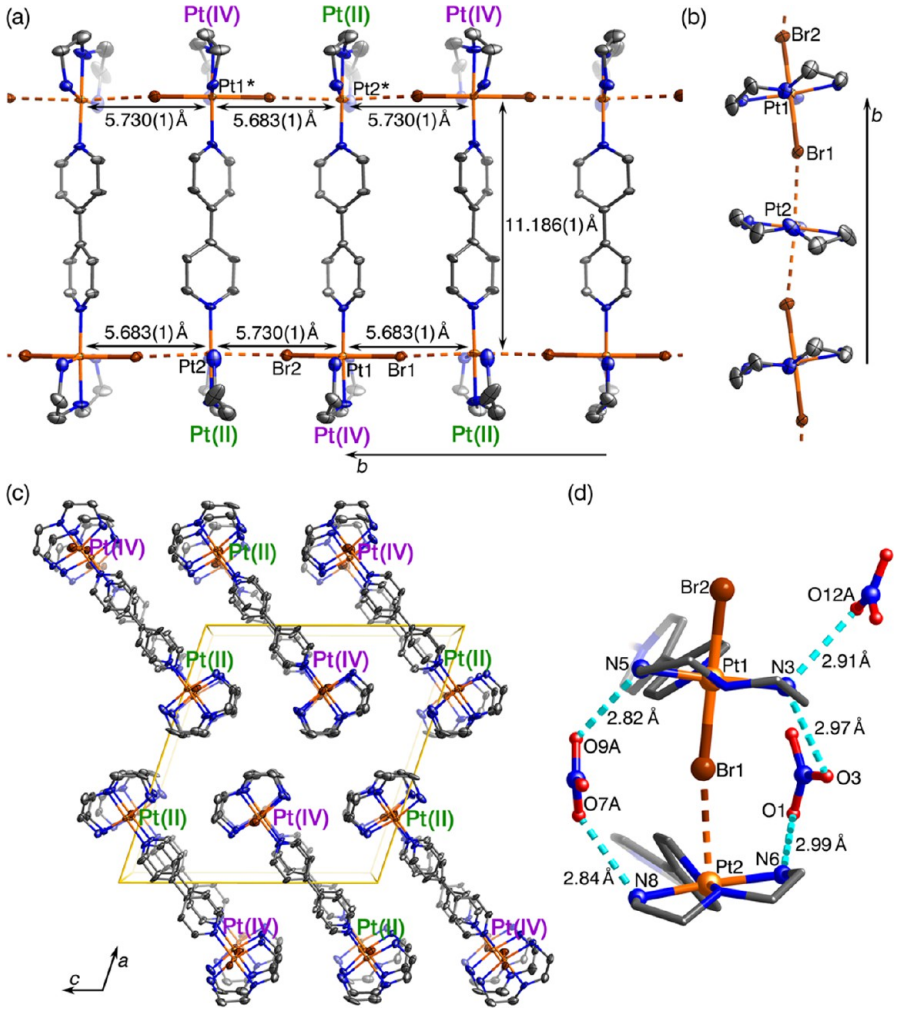

Figure 2. (a) Two-legged ladder structure, (b) MX leg structure from a side view of the ladder, (c) perspective view of 3-D packing, and (d) hydrogen bonds (light-blue dotted lines) between the ladder lattice and NO_3^- of **1** at 100 K. In panels (a), (b), and (c), all water molecules and NO_3^- are omitted for clarity. Pt, C, N, O, and Br atoms are shown in orange, gray, blue, red, and brown, respectively. In panels (a) and (c), the valence states of Pt ions in the same *ab* plane are also shown. Panels (a), (b), and (c) are shown by a thermal ellipsoid model (50% probability).

Crystallographic data in CIF format have been deposited in the Cambridge Crystallographic Data Centre (CCDC) under deposition numbers CCDC-908604 (**1**), CCDC-908605 (**2**), and CCDC-908606 (**3**). These data can be obtained free of charge via www.ccdc.cam.ac.uk/data_request/cif (or from the Cambridge Crystallographic Data Centre, 12 Union Road, Cambridge CB2 1EZ, U.K.).[14]

X-ray Oscillation Photographs. Typical X-ray oscillation photographs of **1**, **2**, and **3** were collected using a Bruker SMART APEX II CCD detector with graphite-monochromated Mo Kα radiation (λ = 0.71073 Å) with ω scan mode (0.3° steps). X-ray oscillation photographs of **2** and **3** at 20 K were collected using a large imaging plate area detector with cold He gas flow installed in the BL02B1 beamline of SPring-8 (λ = 0.6905 Å). The measurements were performed using the ω scan mode (5° steps). Because of heavy sample degradation by radiation damage, full structural analyses of **2** and **3** using synchrotron radiation were not successful.

Diffuse Reflectance Spectroscopy. Diffuse reflectance spectra on **1**, **2**, and **3** diluted in CaF_2 powder were recorded using a JASCO Model ISN-470 60 mm ⌀ integrating-sphere apparatus. The obtained reflectance spectra were converted to absorption spectra according to the Kubelka–Munk function $F(R_\infty)$.

Raman Spectroscopy. Single-crystal Raman spectra on **1**, **2**, and **3** were recorded using a JASCO Model NRS-1000 with a microscope attachment. A Showa Optronics Model JUNO 532-100S Nd:YAG laser (532 nm) provided the exciting line, and each incident laser was polarized parallel to the MX-chain axis.

RESULTS AND DISCUSSION

Syntheses and X-ray Crystal Structures. Novel bromide-bridged two-legged MX ladder compounds $\{[PtBr(dien)]_2(bpy)\}(NO_3)_4\cdot 2H_2O$ (**1**) and $\{[PtBr(dien)]_2(dach)\}(NO_3)_4$ (**2**) were synthesized from binuclear platinum complexes $(\{[Pt(dien)]_2(bpy)\}(NO_3)_4$[6b] and $\{[Pt(dien)]_2(dach)\}(NO_3)_4$, respectively; see Figure S1 in the Supporting Information). Equimolar reactions using each binuclear complex and their brominated complexes produced needle-shaped single crystals suitable for X-ray crystallography of the target two-legged MX-ladder compounds (for details, see the Experimental Section). The crystal structures of **1** and **2** were determined by single-crystal X-ray diffraction (XRD). Two-legged MX ladder **1** crystallizes in the $P2_1/c$ space group. As shown in Figure 2, **1** has a clear two-legged ladder structure,

dx.doi.org/10.1021/ic402846v | Inorg. Chem. 2014, 53, 1229–1240

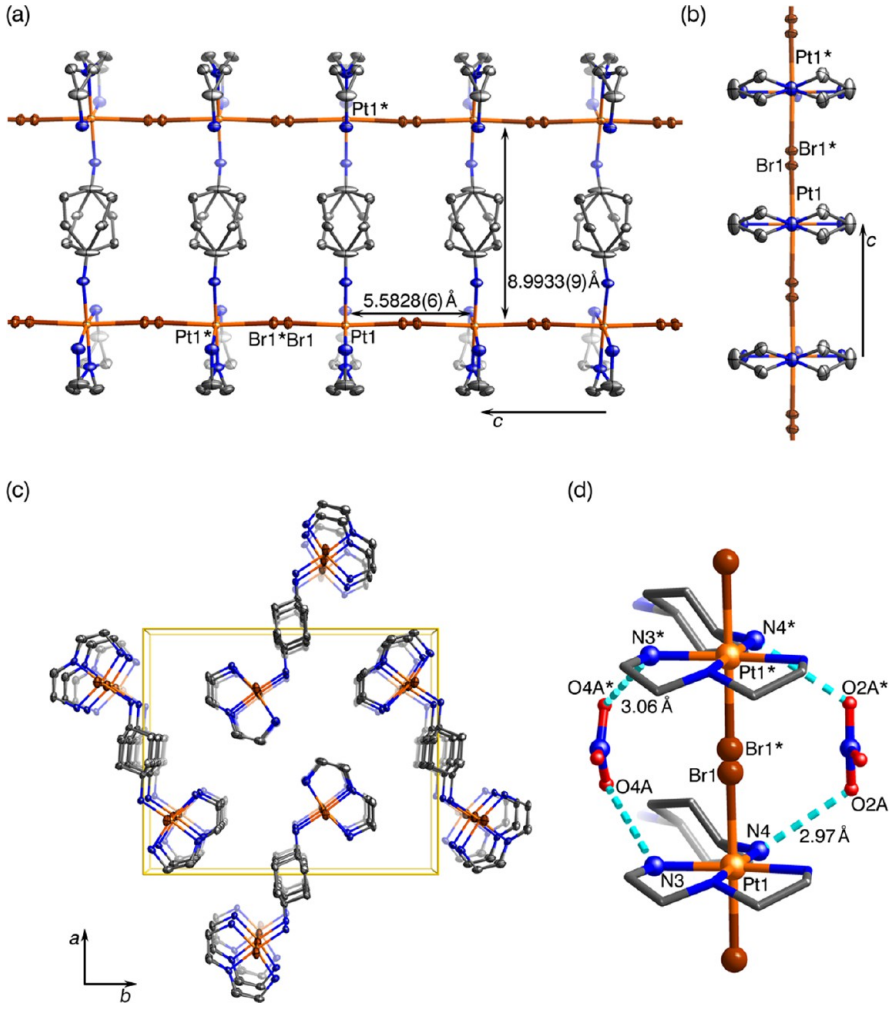

Figure 3. (a) Two-legged ladder structure, (b) MX leg structure from a side view of the ladder, (c) perspective view of 3-D packing, and (d) hydrogen bonds (light-blue dotted lines) between the ladder lattice and NO_3^- anions of **2** at 100 K. In panels (a), (b), and (c), all NO_3^- anions are omitted for clarity. The color setting is the same as in Figure 1. The site occupancy factor of bridging Br^- (Br1) is 0.5. Panels (a), (b), and (c) are shown by a thermal ellipsoid model (50% probability). The dien and dach molecules are disordered with half occupancies.

where two bromide-bridged platinum MX chains constitute its legs. Compound **1** is an analogue of $\{[PtBr(dien)]_2(bpy)\}Br_4 \cdot 2H_2O$,[6b] where the counteranion is NO_3^- instead of Br^-. Interchain separation through the rung bpy is 11.186 Å. The bridging Br^- are well-ordered, deviating from the midpoint between adjacent Pt ions, and there are two crystallographically independent Pt sites in the unit cell, indicating that the electronic state within one MX leg corresponds to the Pt^{II}/Pt^{IV} mixed-valence CDW (···Pt^{II}···Br−Pt^{IV}−Br···) state. As is clearly seen in Figure 2a, all rung bpy and dien units are well-ordered and are arranged with 2-fold periodicity within the ladder. It should be noted that there are two types of Pt−Pt distances along the MX leg (5.730 or 5.683 Å). In the longer Pt−Pt (5.730 Å) part, Pt^{II}···Br (Pt2−Br2) and Pt^{IV}−Br (Pt1−Br2) distances are 3.296 and 2.477 Å, respectively. For the shorter Pt−Pt (5.683 Å) part, Pt^{II}···Br (Pt2−Br1) and Pt^{IV}−Br (Pt1−Br1) distances are 3.213 and 2.487 Å, respectively. Interestingly, a unique "zigzag"-type MX leg quite different from $\{[PtBr(dien)]_2(bpy)\}Br_4 \cdot 2H_2O$ is formed in **1** (Figure 2b), which is the first example of an MX ladder with "zigzag" MX legs.[15] Considering the deviations of each Br^- within the ladder structure of **1**, it was found that a pair of out-of-phase CDWs is achieved, where the opposite site of Pt^{II} along the rung is Pt^{IV}, and vice versa. Compound **1** is the second example of an MX ladder with out-of-phase CDW valence arrangement (the first example is shown in ref 6b). In addition, this valence arrangement of a pair of out-of-phase CDWs is also three-dimensionally ordered between adjacent ladders, where in-phase- and out-of-phase-type arrangements are formed along the *a*- and *c*-axes, respectively, as shown in Figure 2c. NO_3^- anions are located among the adjacent ladders interacting with amine groups of the dien units (O1···N6, O3···N3, O7A···N8, O9A···N5, and O12A···N3) through hydrogen bonds (Figure 2d).

Compound **2** crystallizes in the *Pbam* space group, also having a bromide-bridged two-legged ladder lattice (Figure 3); bridging Br^- are disordered with half occupancies around the midpoint between adjacent Pt ions indicating that the electronic state within one MX leg is also CDW state. In contrast to **1**, there is only one crystallographically independent Pt site; thus, the interchain ordered valence arrangement could not be determined by X-ray crystallography, and all rung (dach) and dien units are disordered. The nearest Pt−Pt distance along the MX leg is 5.583 Å, where Pt^{II}···Br (Pt1*−Br1) and Pt^{IV}−Br (Pt1−Br1) distances are considered to be 3.103 and 2.483 Å, respectively. The rung dach, which has a shorter, distorted

dx.doi.org/10.1021/ic402846v | *Inorg. Chem.* 2014, 53, 1229−1240

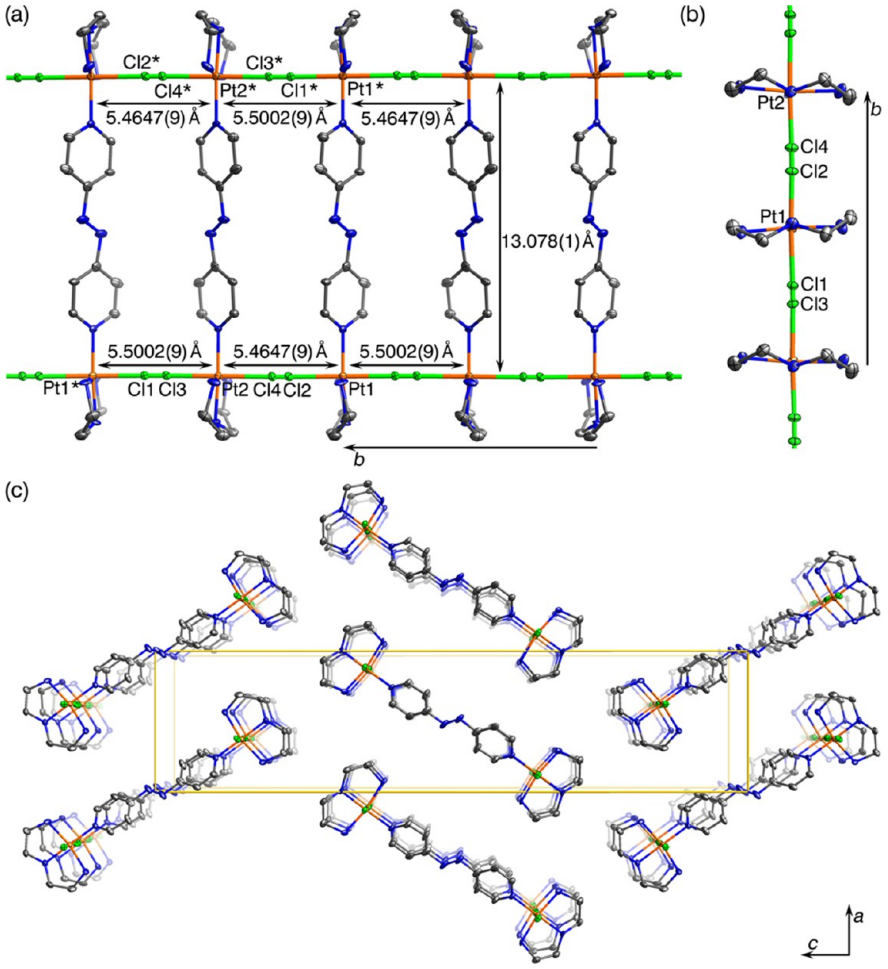

Figure 4. (a) Two-legged ladder structure, (b) MX leg structure from a side view of the ladder, and (c) perspective view of 3-D packing of **3** at 100 K. Each panel is shown by a thermal ellipsoid model (50% probability). All H atoms and crystallization acetone molecules are omitted for clarity. Pt, C, N, and Cl atoms are shown in orange, gray, blue, and light green, respectively. The site occupancy factors of all bridging Cl^- ions (Cl1, Cl2, Cl3, and Cl4) are 0.5.

molecular shape, compared with bpy, provides a shorter interchain Pt−Pt distance along the rung (8.993 Å), and the overall ladder configuration is distorted, resulting in the change in the 3-D packing (Figure 3c). This rung length, 8.993 Å, is a moderate value compared with the other two-legged MX-ladder compounds reported so far, where bpym-bridged MX ladder compounds[6a] have the shortest rung length (∼ 5.47 Å). Note that there is a major difference in the MX leg structure between **1** and **2**. As shown in Figure 3b, **2** has "straight" MX legs similar to other two-legged MX ladder compounds reported to date. This results from the different manner of the hydrogen-bond network between the ladder and NO_3^-; in **1**, NO_3^- anions interact only with amine groups of the dien units to form the hydrogen-bond networks. However, in the case of **2**, they interact strongly not only with dien units (O4A···N3) but also with rung dach units (O2A···N4), resulting in a "straight" leg (Figure 3d).

In a similar manner, the chloride-bridged two-legged MX ladder $\{[PtCl(dien)]_2(azpy)\}(ClO_4)_4\cdot C_3H_6O$ (**3**) was successfully synthesized from $\{[Pt(dien)]_2(azpy)\}(NO_3)_4\cdot 2H_2O$ and $\{[PtCl_2(dien)]_2(azpy)\}(NO_3)_4$ (see Figure S1 in the Supporting Information). Figure 4 shows the crystal structure of **3** confirmed by single-crystal XRD, which revealed that **3** crystallizes in the $P\bar{1}$ space group. Because bridging Cl^- are disordered similar to **2**, the electronic state within one MX leg also corresponds to a CDW state (···Pt^{II}···Cl−Pt^{IV}−Cl···; see Figure 4a). As is clearly seen in Figure 4a, all azpy molecules are well-ordered and are arranged with 2-fold periodicity within the ladder. Interestingly, there are two types of Pt−Pt distances (5.500 and 5.465 Å; see Figure 4a) within the MX leg, indicating that the ladder lattice is slightly distorted, accompanying the periodicity of the ordered azpy. Although these results are similar to those of **1**, distortion of the MX leg of **3** occurs without ordering of the bridging Cl^-. As a result of such a distortion, four types of Pt−Cl distances can be considered. In the longer Pt−Pt (5.500 Å) part, Pt^{II}···Cl (Pt1−Cl3) and Pt^{IV}−Cl (Pt2−Cl3) distances are 3.230 and 2.272 Å, respectively. For the shorter Pt−Pt (5.465 Å) part, Pt^{II}···Cl (Pt1−Cl4) and Pt^{IV}−Cl (Pt2−Cl4) distances are 3.098 and 2.368 Å, respectively. In addition, the rung length of 13.078 Å is the longest value for MX ladder systems reported so far. The ClO_4^- anions are located among the adjacent ladders forming hydrogen-bond networks with amine groups of the dien units (O2···N9, O3···N4, O11A···N7, O12B···N2, O13··N4, and O15···N9) as shown in Figure 5a, and a part of the ClO_4^- anions and acetone molecules are alternately ordered at the sandwich position between the two azpy molecules along the ladder direction (Figure 5b).

Periodic Lattice Distortions of the Two-Legged MX-Ladder Compounds. Figure 6 shows typical X-ray oscillation

dx.doi.org/10.1021/ic402846v | Inorg. Chem. 2014, 53, 1229−1240

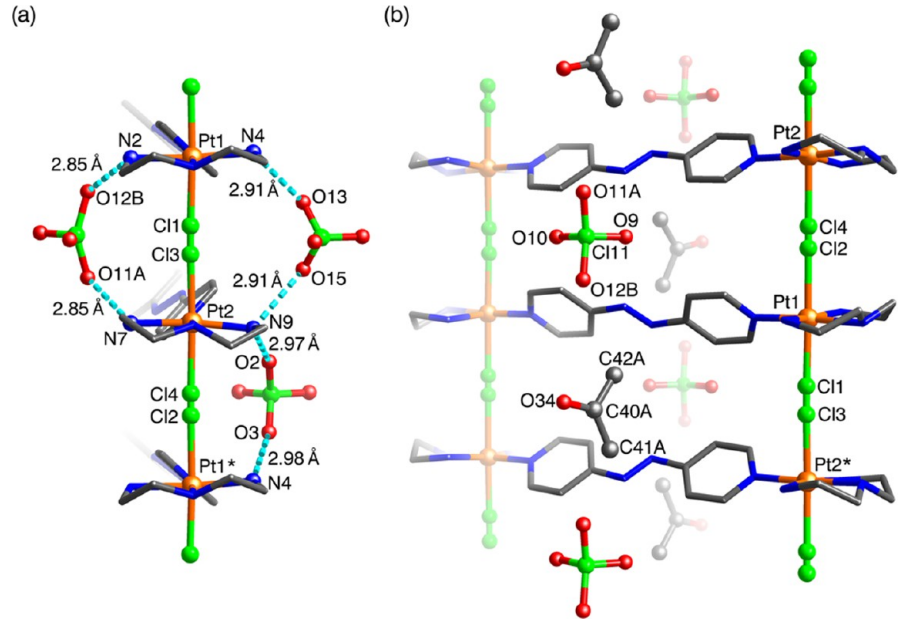

Figure 5. (a) Hydrogen bonds (light-blue dotted lines) between the ladder lattice and ClO_4^-; (b) 2-fold columnar arrangements within the ladder composed of ClO_4^- anions and solvated acetone molecules of **3** at 100 K. Pt, C, N, O, and Cl atoms are shown in orange, gray, blue, red, and light green, respectively. In panel (b), one of the disordered components of the acetone molecule is shown.

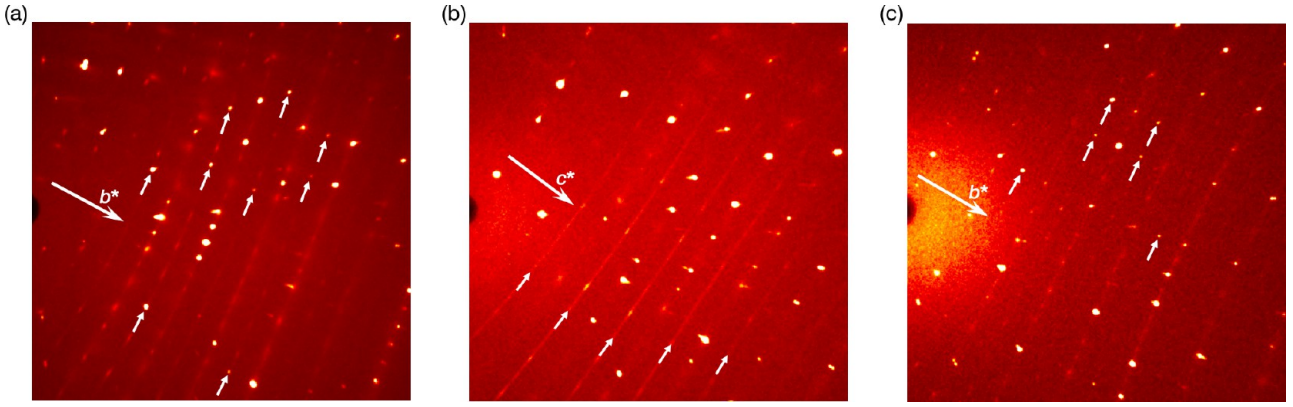

Figure 6. X-ray oscillation photographs of (a) **1**, (b) **2**, and (c) **3** at 100 K. Large arrows in each photograph denote the MX leg axes. Small arrows in each photograph show observed superlattice reflections (panels (a) and (c)) and diffuse scatterings (panel (b)), which are mentioned in the main text.

photographs of **1**, **2**, and **3** at 100 K, which show clear information regarding the electronic states and bridging-halide ions between the adjacent Pt ions within the MX leg. Observation of XRD as spot-type reflections indicates that there is 3-D long-range order within the crystal, whereas diffuse X-ray scattering suggests the existence of some short-range orderings. In the case of **1** and **3** (Figures 6a and 6c), clear superlattice reflections at $hk+{}^1/_2l$ positions derived from 2-fold periodic charge ordering of the CDW state along the b*-axis (MX-leg direction) were observed. In the single-crystal X-ray structural analyses for **1** and **3**, these superlattice reflections were collected and used for refinements. Therefore, compounds **1** and **3** have relatively longer lattice constants along the MX leg direction, which are twice the usual Pt–X–Pt (X = Br, Cl) lengths (see Table 1). In contrast, in the case of **2** (Figure 6b), clear diffuse scatterings at $hkl+{}^1/_2$ positions were observed along the c*-axis (MX leg direction). Such diffuse scatterings were maintained even in the low-temperature region (at 20 K, see Figure S2 in the Supporting Information), and no transition was observed. According to the previous studies on the MX chain family, it is well-known that the observation of superlattice reflections at a 2-fold axis along the MX chain direction indicates the existence of some 3-D ordered structures, including ordering of bridging-halide ions along the chain. As is clearly seen in Figures 2 and 3, all bridging Br^- ions of **1** are 3-D ordered, whereas bridging Br^- ions are disordered in **2**. Although clear superlattice reflections could be observed in **3**, bridging Cl^- ions are completely disordered, and no transition was observed, even at 20 K (see Figure S3 in the Supporting Information). This is because all rung azpy are ordered, resulting in the 2-fold periodicity within the ladder (see Figure 4); therefore, superlattice reflections observed in **3** simply indicate the 3-D ordered rung azpy.

Electronic Properties. To obtain further information about the electronic states of **1**, **2**, and **3**, Raman and diffuse reflectance spectra measurements were performed. As shown in Figure 7, in the Raman spectra of **1**, **2**, and **3**, very strong X–Pt^{IV}–X stretching mode, ν(Pt–X) (X = Br^-, Cl^-), bands with

dx.doi.org/10.1021/ic402846v | Inorg. Chem. 2014, 53, 1229–1240

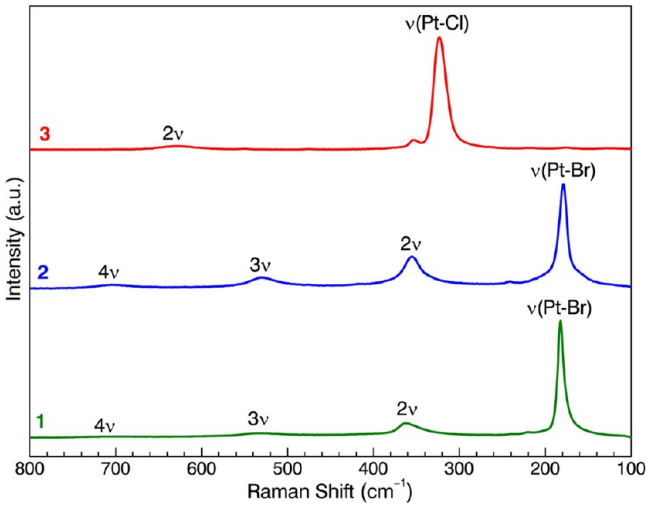

Figure 7. Raman spectra of **1**, **2**, and **3** at room temperature (rt).

its overtone could be observed at 182, 179, and 323 cm^{-1}, respectively. In addition, intense and broad bands that can be assigned as IVCT transitions from the Pt^{II} site to the adjacent Pt^{IV} site within one MX leg were observed at 2.50, 2.33, and 3.60 eV in the diffuse reflectance spectra (Figure 8). Such

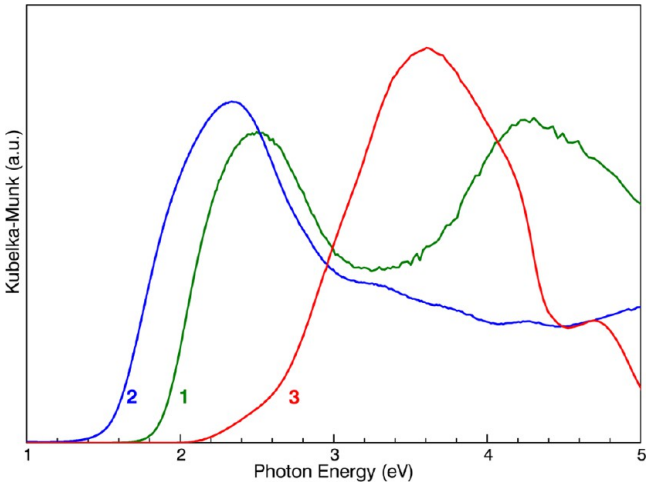

Figure 8. Diffuse reflectance spectra of **1**, **2**, and **3** at rt.

activated overtone progressions observed in the Raman spectra associated with IVCT transition are clear evidence for the mixed-valence CDW state within one MX leg of each of the ladder compounds **1**, **2**, and **3**, and, therefore, each compound corresponds to a Robin–Day class II compound.[16]

Relationship between Lattice Distortion and Electronic Property. It is well-known that the IVCT energy (E_{CT}) of an MX-system strongly depends on the degree of distortion of the bridging-halide ion.[17] The distortion parameter (d) is defined as

$$d = \frac{l_1 - l_2}{L}$$

where l_1, l_2, and L are the $Pt^{II}\cdots X$, $Pt^{IV}-X$, and Pt–Pt distances within the MX chain, respectively. Figure 9 shows the correlation between the d and E_{CT} estimated from optical measurements on several MX chains and two-legged MX ladders reported so far. In the case of a single MX chain system,

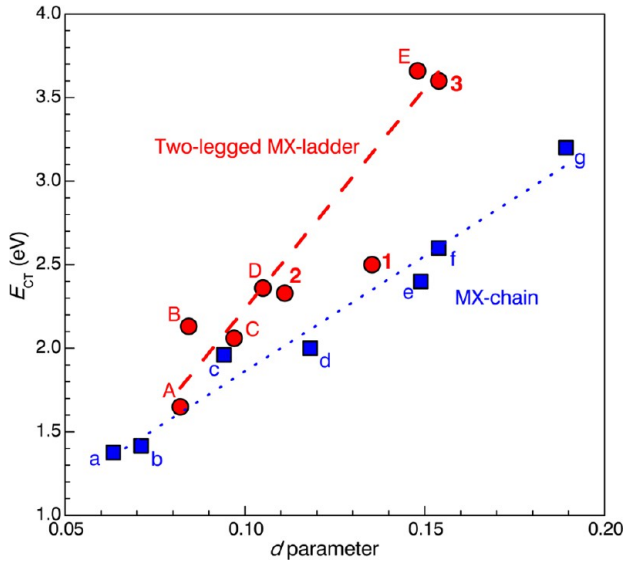

Figure 9. IVCT excitation energies (E_{CT}) plotted against distortion parameter d. Circles (data from the present result and previous reports[6]) denote the data for the two-legged MX ladder system, whereas squares denote the data for the MX chain system.[17] Data shown for $\{[PtI(en)]_2bpym\}I_4\cdot 4H_2O$ (A), $\{[PtBr(dien)]_2bpy\}Br_4\cdot 2H_2O$ (B), $\{[PtBr(en)]_2bpym\}Br_4\cdot 4H_2O$ (C), $\{[PtBr(en)]_2bpym\}Br(ClO_4)_3\cdot H_2O$ (D), $\{[PtCl(en)]_2bpym\}Cl(ClO_4)_3\cdot H_2O$ (E), $[PtI(en)_2](ClO_4)_2$ (a), $[PtBr(chxn)_2]Br_2$ (b), $[PtBr(en)_2](ClO_4)_2$ (c), $[PtBr(etn)_4]Br_2$ (d), $[PtBr(chxn)_2](ClO_4)_2$ (e), $[PtCl(NH_3)_2](HSO_4)_2$ (f), and $[PtCl(chxn)_2](ClO_4)_2$ (g). (For details, see refs 6 and 17.) Dotted and broken lines are guides for the eye (see text).

a linear correlation between the d and E_{CT} can be seen (denoted by the dotted line in Figure 9). As described above, in **1** and **3**, four types of Pt–X distances could be considered within the MX leg. Thus, we estimated the d values from longer and shorter Pt–Pt parts, and used averaged values (d = 0.1354 for **1**, 0.1539 for **3**). As is clearly seen in Figure 9, several important features can be found in the present results. In the cases of **2** and **3**, the E_{CT} values tend to be higher than that of the MX chain, similar to previous two-legged MX ladders. It is worth noting that **3** exhibits an extremely high E_{CT} value, whereas the E_{CT} value of **2** is only slightly elevated. In contrast, the E_{CT} value of **1**, which has a "zigzag" MX leg, is much lower than that of other two-legged MX ladders with "straight" MX legs, and is located close to the trend for the MX chain system. Here, focusing on the trend of the two-legged MX ladder compounds, excluding **1**, a linear correlation between the d and E_{CT} (broken line in Figure 9) with larger slope than that of the single MX chain can also be found. Remarkably, the difference in E_{CT} value between the MX chain and two-legged MX ladder systems becomes larger with increasing d. In addition, it is suggested that the difference in the rung length is not so effective, with regard to the trend of E_{CT} values in the two-legged MX ladder system, compared with the degree of distortion of the MX leg (i.e., d value), because **3**, with the longest rung length (~13.08 Å), exhibits a very similar trend for E_{CT} to the previous chloride-bridged MX ladder with the shortest rung length (~5.47 Å). These results clearly indicate that a very different electronic system is formed in two-legged MX ladder system, compared to a single MX chain system.

According to the extended Peierls–Hubbard model,[18] the E_{CT} value of a two-legged MX ladder with out-of-phase CDW is given by

dx.doi.org/10.1021/ic402846v | Inorg. Chem. 2014, 53, 1229–1240

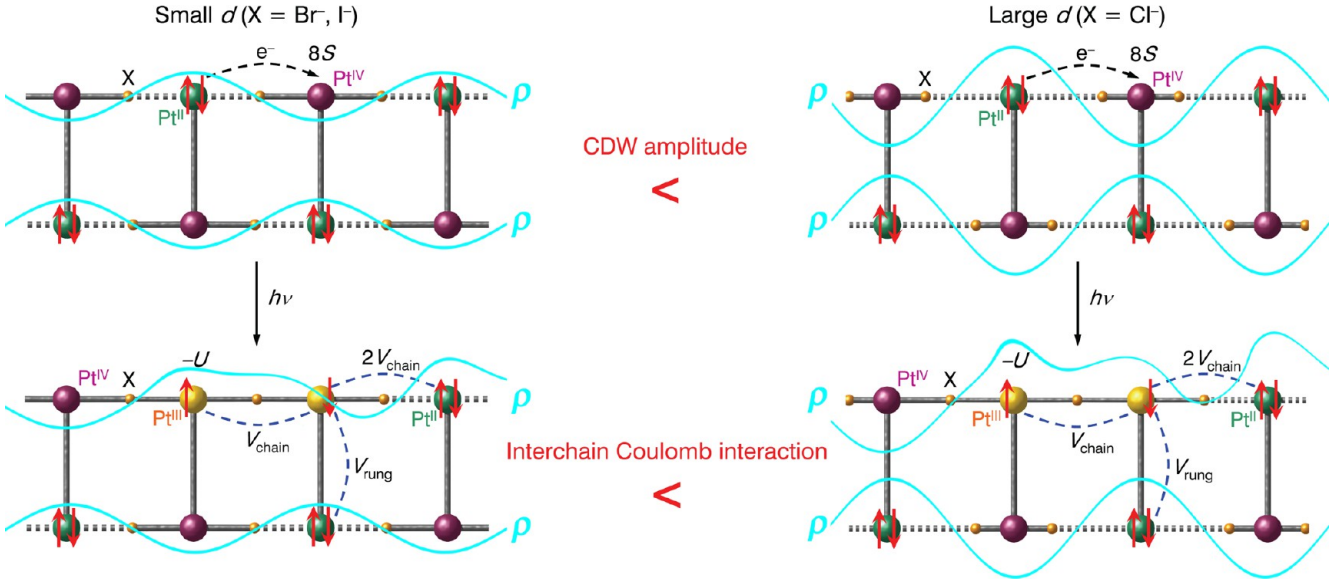

Figure 10. Schematic of the IVCT excitation in a two-legged MX ladder with out-of-phase CDW state based on the extended Peierls–Hubbard model, where the degree of distortion of the MX leg is taken into account (see bridging halide ion sites in each panel). ρ (light-blue wavy lines) denotes the relative degree of CDW considered from distortion of the MX leg. When charge transfer from the Pt^{II} site to the Pt^{IV} site occurs, CDW is modulated because of the realization of Pt^{III} sites (see lower panel). The parameters contributing to E_{CT} on the basis of the extended Peierls–Hubbard model (S, U, V_{chain}, and V_{rung}) are also shown, where $8S$ is the difference in the d_{z^2} energy between the Pt^{II} and Pt^{IV} sites.

$$E_{CT} = 8S - U + 3V_{chain} + 2V_{rung}(\text{out} - \text{of} - \text{phase CDW})$$

where S, U, V_{chain}, and V_{rung} are electron–lattice interaction, onsite and intersite Coulomb repulsions along the one MX leg, and intersite Coulomb repulsion along the rung, respectively.[6b] From recent theoretical studies on two-legged MX ladders,[19] the existence of interchain Coulomb interactions through the rung would explain the relatively high E_{CT} values, compared with those of MX chains (because $V_{rung} = 0$ in the case of a single MX chain).[6b,17−20] Here, we discuss the origin of the distinct tendency of E_{CT} in two-legged MX ladder system with "straight" MX legs including **2** and **3**, as shown in Figure 9. Considering the degree of distortion of the MX leg, the valence structure of the CDW state within one leg can be formally written as

$$\cdots Pt^{3-\delta}\cdots X{-}Pt^{3+\delta}{-}X\cdots Pt^{3-\delta}\cdots X{-}Pt^{3+\delta}{-}X\cdots \quad (0 < \delta \leq 1)$$

where δ corresponds to the d (i.e., amplitude of the CDW). Figure 10 shows a schematic of the CT excitation in a two-legged MX ladder with an out-of-phase CDW state based on the extended Peierls–Hubbard model, where the degree of distortion of the MX leg is taken into account. In the smaller d region (X = Br^- and I^-, δ is relatively small), the CDW amplitude within each MX leg can be considered to be small, and, therefore, the intersite Coulomb repulsion between adjacent chains within the ladder (V_{rung}) is expected to become weaker upon CT excitation. On the other hand, in the case of the larger d region (X = Cl^-, δ is relatively large), the large CDW amplitude within each MX leg might provide strong V_{rung}, resulting in an extremely high E_{CT} value. Because the CDW amplitude corresponds to the degree of localization of the charge on the Pt site (i.e., distinctiveness of Pt^{II} and Pt^{IV} sites), the relative strength of the V_{rung} is dominated by the CDW amplitude, and as a result, a distinct trend of the E_{CT} value in the two-legged MX-ladder system might be observed. In the case of an in-phase CDW state, a similar model with shifted CDW can be considered, where intersite Coulomb repulsion through the rung, V_{rung} is replaced with intersite Coulomb repulsion in a diagonal direction, V_{diag}.[6a,19a,20] Because the bridging-halide ions are disordered in **2** and **3**, their valence arrangements have not been identified at the present stage (such as in-phase or out-of-phase CDW); however, the CDW amplitude derived from the distortion within the MX leg would play an important role in dominating the interchain Coulomb interactions in both cases. Because **1** has "zigzag"-shaped MX legs, which are very different from the other two-legged MX ladder compounds with "straight" MX legs, a mismatch of the CDW amplitudes (see Figure 10) between the MX legs might occur and Coulomb repulsion along the leg (i.e., V_{chain}) might become weaker, resulting in a low E_{CT}.

CONCLUSIONS

In conclusion, we have successfully fabricated three novel halogen-bridged two-legged MX ladder compounds composed of the organic rung units, bpy, dach, and azpy, each with varying molecular size and shape. Single-crystal X-ray studies showed that each ladder compound is composed of MX chains as its legs, and the overall 3-D two-legged ladder configuration strongly depends on the geometry of the rung. The MX leg distortion, which was derived from the CDW state, also strongly depends on the rung variation, which results in characteristic E_{CT} values. In addition, by increasing the variation of the compounds, we have successfully demonstrated, for the first time, that the two-legged MX ladder system shows a distinct correlation of the IVCT band gaps with the degree of distortion of the constituent leg. The organic rung in the two-legged MX ladder system creates a distinctive electronic system compared with the single MX chain system, while also allowing for systematic modifications through substitution of the rung. The results presented here provide useful insights into a wide

dx.doi.org/10.1021/ic402846v | Inorg. Chem. 2014, 53, 1229−1240

and rational tunability of physical and electronic properties based on the dimensional control not only of ladder materials but also of future metal complex-based nanomaterials.

■ ASSOCIATED CONTENT

Supporting Information

Figures S1−S3, experimental and refinement details of single-crystal X-ray crystallography, crystallographic data in CIF format. This material is available free of charge via the Internet at http://pubs.acs.org.

■ AUTHOR INFORMATION

Corresponding Authors

*E-mail: kazuya@kuchem.kyoto-u.ac.jp (K. Otsubo).
*E-mail: kitagawa@kuchem.kyoto-u.ac.jp (H. Kitagawa).

Notes

The authors declare no competing financial interest.

■ ACKNOWLEDGMENTS

This work was partly supported by Grants-in-Aid for Scientific Research (A) (Nos. 20350030 and 23245012), Grant-in-Aid for Young Scientists (B) (No. 25810039) from JSPS and a Grant-in-Aid for the Global COE Program, "Science for Future Molecular Systems" from MEXT. Synchrotron XRD measurements were supported by the Japan Synchrotron Radiation Research Institute (JASRI) (Proposal Nos. 2011B1575 and 2012A1504).

■ REFERENCES

(1) (a) Day, P. Molecules into Materials: *Case Studies in Materials Chemistry−Mixed Valency, Magnetism and Superconductivity*; World Scientific Publishing: Singapore, 2007. (b) Tokura, Y.; Yaguchi, Y.; Okada, Y.; Fujishima, Y.; Arima, T.; Kumagai, K.; Irie, Y. *Phys. Rev. Lett.* **1993**, *70*, 2126. (c) Bednorz, J. G.; Müller, K. A. *Z. Phys. B* **1986**, *64*, 189. (d) Heeger, A. J. In *Highly Conducting One-Dimensional Solids*, Devrees, T. J.; Evrand, P. R.; van Doren, E. V., Eds.; Plenum: New York, 1979; p 69. (e) Overhauser, W. A. *Phys. Rev.* **1963**, *128*, 1437.

(2) (a) Krogmann, K. *Angew. Chem., Int. Ed. Engl.* **1969**, *8*, 35. (b) Kuse, D.; Zeller, R. H. *Phys. Rev. Lett.* **1971**, *27*, 1060. (c) Williams, M. J.; Schultz, J. A.; Underhill, A. E.; Carneiro, K. In *Extended Linear Chain Compounds*; Miller, J. S., Ed.; Plenum Press: New York, 1982; Vol. *1*, p 73. (d) Bechgaard, K.; Jacobsen, S. C.; Mortensen, K.; Pedersen, H. J.; Throrup, N. *Solid State Commun.* **1980**, *33*, 1119. (e) Ferraris, J.; Cowan, D. O.; Walatke, V.; Perlstein, J. H., Jr. *J. Am. Chem. Soc.* **1973**, *95*, 948. (f) Cohen, J. M.; Coleman, B. L.; Garito, F. A.; Heeger, J. A. *Phys. Rev. B* **1974**, *10*, 1298. (g) Mott, F. N. *Metal−Insulator Transitions*; Taylor and Francis: London, 1974. (h) Peierls, E. R. *Quantum Theory of Solids*; Clarendon Press: Oxford, U.K., 1974. (i) Goldberg, I. B.; Crowe, H. R.; Newman, P. R.; Heeger, A. J.; MacDiarmid, A. G. *J. Chem. Phys.* **1979**, *70*, 1132. (j) Kitagawa, H.; Onodera, N.; Sonoyama, T.; Yamamoto, M.; Fukawa, T.; Mitani, T.; Seto, M.; Maeda, Y. *J. Am. Chem. Soc.* **1999**, *121*, 10068. (k) Mitsumi, M.; Murase, T.; Kishida, H.; Yoshinari, T.; Ozawa, Y.; Toriumi, K.; Sonoyama, T.; Kitagawa, H.; Mitani, T. *J. Am. Chem. Soc.* **2001**, *123*, 11179.

(3) (a) Azuma, M.; Hiroi, Z.; Takano, M.; Ishida, K.; Kitaoka, Y. *Phys. Rev. Lett.* **1994**, *73*, 3463. (b) Hiroi, Z.; Takano, M. *Nature* **1995**, *377*, 41. (c) Uehara, M.; Nagata, T.; Akimitu, J.; Takahashi, H.; Mori, N.; Kinoshita, K. *J. Phys. Soc. Jpn.* **1996**, *65*, 2764. (d) Blumberg, G.; Littlewood, P.; Gozar, A.; Dennis, B. S.; Motoyama, N.; Eisaki, H.; Uchida, S. *Science* **2002**, *297*, 584. (e) Abbamonte, P.; Blumberg, G.; Rusydi, A.; Gozar, A.; Evans, P. G.; Siegrist, T.; Venema, L.; Eisaki, H.; Isaacs, E. D.; Sawatzky, G. A. *Nature* **2004**, *431*, 1078. (f) Lake, B.; Tsvelik, A. M.; Notbohm, S.; Tennant, D. A.; Perring, T. G.; Reehuis, M.; Sekar, C.; Krabbes, G.; Büchner, B. *Nat. Phys.* **2009**, *6*, 50. (g) Damay, F.; Martin, C.; Hardy, V.; Maignan, A.; Stock, C.; Petit, S. *Phys. Rev. B* **2011**, *84*, 020402. (h) Thorsmølle, V. K.; Homes, C. C.; Gozar, A.; Blumberg, G.; van Mechelen, J. L. M.; Kuzmenko, A. B.; Vanishri, S.; Marin, C.; Rønnow, H. M. *Phys. Rev. Lett.* **2012**, *108*, 217401.

(4) (a) Yaghi, O. M.; O'Keeffe, M.; Ockwig, N. W.; Chae, H. K.; Eddaoudi, M.; Kim, J. *Nature* **2003**, *423*, 705. (b) Kitagawa, S.; Kitaura, R.; Noro, S. *Angew. Chem., Int. Ed.* **2004**, *43*, 2334. (c) Fujita, M.; Tominaga, M.; Hori, A.; Therrien, B. *Acc. Chem. Res.* **2005**, *38*, 371. (d) Ferey, G. *Chem. Soc. Rev.* **2008**, *37*, 191.

(5) (a) Matsumoto, N.; Yamashita, M.; Kida, S. *Bull. Chem. Soc. Jpn.* **1978**, *51*, 2334. (b) Keller, H. J.; Martin, D. S., Jr. In *Extended Linear Chain Compounds*; Miller, J. S., Ed.; Plenum Press: New York, 1982; Vol. *1*, p 357. (c) Clark, R. J. H.; Kurmoo, M.; Galas, A. M. R.; Hursthouse, M. B. *J. Chem. Soc., Dalton Trans.* **1983**, 1583. (d) Tanino, H.; Kobayashi, K. *J. Phys. Soc. Jpn.* **1983**, *52*, 1446. (e) Okamoto, H.; Mitani, T.; Toriumi, K.; Yamashita, M. *Phys. Rev. Lett.* **1992**, *69*, 2248. (f) Scott, B.; Love, S. P.; Kanner, G. S.; Johnson, S. R.; Wilkerson, M. P.; Berkey, M.; Swanson, B. I.; Sexena, A.; Huang, X. Z.; Bishop, A. R. *J. Mol. Struct.* **1995**, *356*, 207. (g) Kimura, N.; Ishimaru, S.; Ikeda, R.; Yamashita, M. *J. Chem. Soc., Faraday Trans.* **1998**, *94*, 3659. (h) Yamashita, M.; Ishii, T.; Matsuzaka, H.; Manabe, T.; Kawashima, T.; Okamoto, H.; Kitagawa, H.; Mitani, T.; Marumoto, K.; Kuroda, S. *Inorg. Chem.* **1999**, *38*, 5124. (i) Kishida, H.; Matsuzaki, H.; Okamoto, H.; Manabe, T.; Yamashita, M.; Taguchi, Y.; Tokura, Y. *Nature* **2000**, *405*, 929. (j) Takaishi, S.; Miyasaka, H.; Sugiura, S.; Yamashita, M.; Matsuzaki, H.; Kishida, H.; Okamoto, H.; Tanaka, H.; Marumoto, K.; Ito, H.; Kuroda, S.; Takami, T. *Angew. Chem., Int. Ed.* **2004**, *43*, 3171. (k) Sasaki, M.; Takaishi, S.; Miyasaka, H.; Sugiura, K.; Yamashita, M. *J. Am. Chem. Soc.* **2005**, *127*, 14958. (l) Takaishi, S.; Takamura, M.; Kajiwara, T.; Miyasaka, H.; Yamashita, M.; Iwata, M.; Matsuzaki, H.; Okamoto, H.; Tanaka, H.; Kuroda, S.; Nishikawa, H.; Oshio, H.; Kato, K.; Takata, M. *J. Am. Chem. Soc.* **2006**, *128*, 6420. (m) Takaishi, S.; Takamura, M.; Kajiwara, T.; Miyasaka, H.; Yamashita, M.; Iwata, M.; Matsuzaki, H.; Okamoto, H.; Kato, K.; Takata, M. *J. Am. Chem. Soc.* **2008**, *130*, 12080. (n) Kimura, K.; Matsuzaki, H.; Takaishi, S.; Yamashita, M.; Okamoto, H. *Phys. Rev. B* **2009**, *79*, 075116. (o) Iguchi, H.; Takaishi, S.; Jiang, D.; Xie, J.; Yamashita, M.; Uchida, A.; Kawaji, H. *Inorg. Chem.* **2013**, *52*, 13812.

(6) (a) Kawakami, D.; Yamashita, M.; Matsunaga, S.; Takaishi, S.; Kajiwara, T.; Miyasaka, H.; Sugiura, K.; Matsuzaki, H.; Okamoto, H.; Wakabayashi, Y.; Sawa, H. *Angew. Chem., Int. Ed.* **2006**, *45*, 7214. (b) Kobayashi, A.; Kitagawa, H. *J. Am. Chem. Soc.* **2006**, *128*, 12066. (c) Yamada, T.; Otsubo, K.; Makiura, R.; Kitagawa, H. *Chem. Soc. Rev.* **2013**, *42*, 6655.

(7) Otsubo, K.; Wakabayashi, Y.; Ohara, J.; Yamamoto, S.; Matsuzaki, H.; Okamoto, H.; Nitta, K.; Uruga, T.; Kitagawa, H. *Nat. Mater.* **2011**, *10*, 291.

(8) See the Supporting Information.

(9) Burla, M. C.; Caliandro, R.; Camalli, M.; Carrozzini, B.; Cascarano, G. L.; De Caro, L.; Giacovazzo, C.; Polidori, G.; Spagana, R. *J. Appl. Crystallogr.* **2005**, *38*, 381.

(10) Altomare, A.; Cascarano, G.; Giacovazzo, C.; Guagliardi, A.; Burla, M.; Polidori, G.; Camalli, M. *J. Appl. Crystallogr.* **1994**, *27*, 435.

(11) Beurskens, P. T.; Admiraal, G.; Beurskens, G.; Bosman, W. P.; de Gelder, R.; Israel, R.; Smits, J. M. M. *DIRDIF99*; Crystallography Laboratory, University of Nijmegen:: The Netherlands, 1999.

(12) Sheldrick, G. M. *Acta Crystallogr., Sect. A: Found. Crystallogr.* **2008**, *64*, 112.

(13) *CrystalStructure 3.8.0: Crystal Structure Analysis Package*; Rigaku and Rigaku/MSC, 2000−2006.

(14) Crystallographic data regarding this paper have been deposited with the Cambridge Crystallographic Data Centre as CCDC-908601−CCDC-908606.

(15) An example of a single MX-chain compound with such a "zigzag" chain structure was reported in ref 5c.

(16) Robin, M. B.; Day, P. *Inorg. Chem. Radiochem.* **1967**, *9*, 247.

(17) Okamoto, H.; Mitani, T.; Toriumi, K.; Yamashita, M. *Mater. Sci. Eng., B* **1992**, *13*, L9.

(18) (a) Iwano, K. *J. Phys. Soc. Jpn.* **1997**, *66*, 1088. (b) Matsuzaki, H.; Iwano, K.; Aizawa, T.; Ono, M.; Kishida, H.; Yamashita, M.; Okamoto, H. *Phys. Rev. B* **2004**, *70*, 035204. (c) Iwano, K. Presented at *The Annual Meeting of the Physical Society of Japan*, Paper No. 27pYK-5, Noda, Japan, 2005.
(19) (a) Yamamoto, S.; Ohara, J. *Phys. Rev. B* **2007**, *76*, 235116. (b) Iwano, K.; Shimoi, Y. *J. Phys. Soc. Jpn.* **2007**, *76*, 063708. (c) Ohara, J.; Yamamoto, S. *Europhys. Lett.* **2009**, *87*, 17006.
(20) In a similar manner, the E_{CT} value for the in-phase CDW type valence arrangement (compound D in Figure 9 in ref 6a) can be given by $E_{CT} = 8S - U + 3\,V_{chain} + 4V_{diag} - 2V_{rung}$ (in phase CDW), where V_{diag} is the intersite Coulomb repulsion in the diagonal direction within the ladder. In this case, interchain Coulomb repulsions also play an important role in determining the E_{CT} value. For details, see refs 6 and 19.

dx.doi.org/10.1021/ic402846v | *Inorg. Chem.* 2014, 53, 1229−1240